J|A|C|S
ARTICLES
Published on Web 12/09/2006

Hydrogen Storage in a Microporous Metal−Organic Framework with Exposed Mn^{2+} Coordination Sites

Mircea Dincă,[†] Anne Dailly,[‡,⊥] Yun Liu,[§,||] Craig M. Brown,[§,#] Dan. A. Neumann,[§] and Jeffrey R. Long*[,†]

Contribution from the Department of Chemistry, University of California, Berkeley, California 94720, Chemical and Environmental Sciences Laboratory, General Motors Corporation, Warren, Michigan 48090, College of Engineering, Purdue University, West Lafayette, Indiana 47907, Center for Neutron Research, National Institute of Standards and Technology, Gaithersburg, Maryland 20899, Department of Materials Science and Engineering, University of Maryland, College Park, Maryland 20742, and Indiana University Cyclotron Facility, Bloomington, Indiana 47408

Received August 5, 2006; E-mail: jrlong@berkeley.edu

Abstract: Use of the tritopic bridging ligand 1,3,5-benzenetristetrazolate (BTT^{3-}) enables formation of $[Mn(DMF)_6]_3[(Mn_4Cl)_3(BTT)_8(H_2O)_{12}]_2 \cdot 42DMF \cdot 11H_2O \cdot 20CH_3OH$, featuring a porous metal−organic framework with a previously unknown cubic topology. Crystals of the compound remain intact upon desolvation and show a total H_2 uptake of 6.9 wt % at 77 K and 90 bar, which at 60 g H_2/L provides a storage density 85% of that of liquid hydrogen. The material exhibits a maximum isosteric heat of adsorption of 10.1 kJ/mol, the highest yet observed for a metal−organic framework. Neutron powder diffraction data demonstrate that this is directly related to H_2 binding at coordinatively unsaturated Mn^{2+} centers within the framework.

Introduction

The utilization of hydrogen in automobiles as a clean-burning substitute for fossil fuels relies in part upon the development of a viable on-board storage system.[1,2] Recently, a new class of ordered, three-dimensional extended solids composed of metal ions and organic linkers, known as metal−organic frameworks, has emerged as a promising storage alternative to high-pressure and liquefied hydrogen tanks, metal hydrides, and carbon-based adsorbents.[3−25] Due to their porous nature and unusually high surface areas, these new materials show exceptional H_2 uptake by mass but are also characterized by very weak H_2 adsorption energies (typically 4−7 kJ/mol), such that cryogenic temperatures are required to observe significant H_2 uptake. Clearly, frameworks exhibiting stronger binding interactions are needed to facilitate H_2 adsorption at higher temperatures; indeed, a binding energy of 15 kJ/mol has been predicted to maximize the amount of adsorbed H_2 accessible at 298 K within the pressure range 1.5−20 bar.[26]

Two main strategies have been pursued for enhancing H_2 binding within metal−organic frameworks. First, by forming frameworks with very narrow pores, wherein overlapping potentials from two or more pore walls interact with a single H_2 molecule, H_2 binding energies of up to 9.5 kJ/mol have been observed.[15] More promisingly, it has been proposed that the

[†] University of California, Berkeley.
[‡] General Motors Corp.
[⊥] Purdue University.
[§] NIST Center for Neutron Research.
[||] University of Maryland.
[#] Indiana University Cyclotron Facility.

(1) Schlapbach, L.; Züttel, A. *Nature* **2001**, *414*, 353−358.
(2) EERE: Hydrogen, Fuel Cells, & Infrastructure Technologies Program Homepage, www.eere.energy.gov/hydrogenandfuelcells/ (2006).
(3) Rosi, N. L.; Eckert, J.; Eddaoudi, M.; Vodak, D. T.; Kim, J.; O'Keeffe, M.; Yaghi, O. M. *Science* **2003**, *300*, 1127−1129.
(4) Férey, G.; Latroche, M.; Serre, C.; Millange, F.; Loiseau, T.; Percheron-Guégan, A. *Chem. Commun.* **2003**, 2976−2977.
(5) Dybtsev, D. N.; Chun, H.; Kim, K. *Angew. Chem., Int. Ed.* **2004**, *43*, 5033−5036.
(6) Rowsell, J. L.; Millward, A. R.; Park, K. S.; Yaghi, O. M. *J. Am. Chem. Soc.* **2004**, *126*, 5666−5667.
(7) Zhao, X.; Xiao, B.; Fletcher, A. J.; Thomas, K. M.; Bradshaw, D.; Rosseinsky, M. J. *Science* **2004**, *306*, 1012−1015.
(8) Dybtsev, D. N.; Chun, H.; Yoon, S. H.; Kim, D.; Kim, K. *J. Am. Chem. Soc.* **2004**, *126*, 32−33.
(9) Pan, L.; Sander, M. B.; Huang, X.; Li, J.; Smith, M.; Bittner, E.; Bockrath, B.; Johnson, J. K. *J. Am. Chem. Soc.* **2004**, *126*, 1308−1309.
(10) Lee, E. Y.; Suh, M. P. *Angew. Chem., Int. Ed.* **2004**, *43*, 2798−2801.
(11) Kesanli, B.; Cui, Y.; Smith, M. R.; Bittner, E. W.; Bockrath, B. C.; Lin, W. *Angew. Chem., Int. Ed.* **2005**, *44*, 72−75.
(12) Kubota, Y.; Takata, M.; Matsuda, R.; Kitaura, R.; Kitagawa, S.; Kato, K.; Sakata, M.; Kobayashi, T. C. *Angew. Chem., Int. Ed.* **2005**, *44*, 920−923.
(13) Chun, H.; Dybtsev, D. N.; Kim, H.; Kim, K. *Chem.-Eur. J.* **2005**, *11*, 3521−3529.
(14) Chen, B.; Ockwig, N. W.; Millward, A. R.; Contreras, D. S.; Yaghi, O. M. *Angew. Chem., Int. Ed.* **2005**, *44*, 4745−4749.
(15) Dinca, M.; Long, J. R. *J. Am. Chem. Soc.* **2005**, *127*, 9376−9377.
(16) Lee, J.-Y.; Li, J.; Jagiello, J. *J. Solid State Chem.* **2005**, *178*, 2527−2532.
(17) Lee, J.-Y.; Pan, L.; Kelly, S. R.; Jagiello, J.; Emge, T. J.; Li, J. *Adv. Mater.* **2005**, *17*, 2703−2706.
(18) Wong-Foy, A. G.; Matzger, A. J.; Yaghi, O. M. *J. Am. Chem. Soc.* **2006**, *128*, 3494−3495.
(19) Dinca, M.; Yu, A. F.; Long, J. R. *J. Am. Chem. Soc.* **2006**, *128*, 8904−8913.
(20) Sun, D.; Ma, S.; Ke, Y.; Collins, D. J.; Zhou, H.-C. *J. Am. Chem. Soc.* **2006**, *128*, 3896−3897.
(21) Rowsell, J. L. C.; Yaghi, O. M. *J. Am. Chem. Soc.* **2006**, *128*, 1304−1315.
(22) Chen, B. L.; Ma, S. Q.; Zapata, F.; Lobkovsky, E. B.; Yang, J. *Inorg. Chem.* **2006**, *45*, 5718−5720.
(23) Dailly, A.; Vajo, J. J.; Ahn, C. C. *J. Phys. Chem. B* **2006**, *110*, 1099−1101.
(24) Park, K. S.; Ni, Z.; Côté, A. P.; Choi, J. Y.; Huang, R.; Uribe-Romo, F. J.; Chae, H. K.; O'Keeffe, M.; Yaghi, O. M. *Proc. Natl. Acad. Sci. U.S.A.* **2006**, *103*, 10186−10191.
(25) Li, Y. W.; Yang, R. T. *J. Am. Chem. Soc.* **2006**, *128*, 726−727.

10.1021/ja0656853 CCC: $33.50

presence of coordinatively unsaturated metal centers could increase the affinity for H_2 through strong metal−H_2 interactions.[14,27,28] Our strategy has involved the use of polytetrazolate bridging ligands with an N donor atom arrangement deemed favorable for creating rigid frameworks with exposed metal coordination sites.[19] The present work demonstrates the success of this approach, with use of 1,3,5-benzenetristetrazolate (BTT^{3-}) in producing a stable, microporous material exhibiting a high surface area and exceptional H_2 uptake. Moreover, neutron powder diffraction is employed to confirm that the high H_2 adsorption enthalpy observed for this material is due to H_2 binding directly to unsaturated metal centers within the pores of the framework.

Experimental Section

All reagents were obtained from commercial vendors and, unless otherwise noted, were used without further purification. Methanol was distilled over Mg/I_2 prior to use.

1,3,5-Tris(2*H*-tetrazol-5-yl)benzene Hydrochloride ($H_3BTT\cdot 2HCl$). A mixture of 1,3,5-tricyanobenzene[29] (3.06 g, 20.0 mmol), NaN_3 (11.7 g, 180 mmol), and triethylamine hydrochloride (24.7 g, 180 mmol) in 150 mL of toluene and 30 mL of methanol was heated at reflux in a 500-mL round-bottom flask for 3 days. Upon cooling to room temperature, 100 mL of an aqueous solution of NaOH (1 M) was added, and the mixture was stirred for 30 min. The aqueous layer was treated with ca. 100 mL of diluted HCl (1 M) until no further white precipitate formed. The precipitate was then collected by filtration, dried in the air, and dissolved in aqueous NaOH (1 M). The resulting clear, colorless solution was titrated with ca. 75 mL of diluted HCl (1 M) until the pH of the solution was 4−5. The ensuing white precipitate was washed with successive aliquots of distilled water (3 × 50 mL), methanol (2 × 50 mL), and acetone (50 mL) to afford 7.1 g (87%) of product. Anal. Calcd for $C_9H_6N_{12}\cdot 2HCl\cdot H_2O\cdot CH_3OH$: C, 29.64; H, 3.48; N, 41.48. Found: C, 29.84; H, 3.49; N, 41.84. IR (neat): 3347 (s, br), 3066 (m), 2329 (m, br), 1889 (m, br), 1636 (m, br), 1430 (s), 1409 (s), 1377 (s), 1321 (w), 1204 (m), 1176 (m), 1116 (m), 1053 (s), 896 (s), 746 (s) cm^{-1}. ^1H NMR (dmso-d_6): δ 8.79 ppm (s, 3H). This compound is soluble in DMF and dimethylsulfoxide but is insoluble in nonpolar organic solvents; it can be recrystallized from hot methanol or hot water.

Caution! Metal azides are water sensitive and potentially explosive and should be handled with care. Although we did not encounter any incidents while handling H_3BTT or compounds **1**, **1′**, **1m**, and **1m′** under the conditions of our experiments, previous reports suggest that handling H_3BTT at temperatures above 160 °C is potentially unsafe and that melting with decomposition (explosion) occurs at 280 °C.[29]

$[Mn(DMF)_6]_3[(Mn_4Cl)_3(BTT)_8(H_2O)_{12}]_2\cdot 42DMF\cdot 11H_2O\cdot 20CH_3OH$ (1). A solution of $MnCl_2\cdot 4H_2O$ (200 mg, 1.0 mmol) in 5 mL of methanol was added to a solution of $H_3BTT\cdot 2HCl\cdot H_2O\cdot CH_3OH$ (45 mg, 0.11 mmol) in 5 mL of DMF in a Teflon-capped 20-mL scintillation vial. The pH of the solution was then adjusted to ca. 3 using an aqueous solution of HCl (1 M), and the resulting mixture was heated to 70 °C. Colorless cube-shaped crystals suitable for X-ray analysis were collected from the walls of the vial after 24 h. The crystals were collected by filtration, washed with successive 20-mL aliquots of DMF and methanol, and then quickly dried on a piece of filter paper to afford 65 mg (40%) of product. Anal. Calcd for $C_{344}H_{618}Cl_6Mn_{27}N_{252}O_{115}$: C, 34.95; H, 5.27; N, 29.86. Found: C, 34.81; H, 4.97; N, 30.15. IR (neat): 1651 (s), 1414 (m), 1387 (w), 1101 (w), 790 (m), 749 (w), 675 (w) cm^{-1}. The solvent content of this compound was confirmed by thermogravimetric analysis (TGA), and phase purity was confirmed by powder X-ray diffraction. Crystals of **1** become opaque after prolonged exposure to the atmosphere and were therefore stored under dinitrogen. The partially desolvated form of this compound, $[Mn(DMF)_6]_3[(Mn_4Cl)_3(BTT)_8(DMF)_{12}]_2$ (**1′**), was generated by heating **1** at 150 °C under dynamic vacuum for a minimum of 2 h.

$[Mn(CH_3OH)_6]_3[(Mn_4Cl)_3(BTT)_8(CH_3OH)_{12}]_2\cdot 42CH_3OH$ (1m). Crystals of **1** were immersed in freshly distilled methanol and soaked for 1 day inside an N_2-filled glovebag. The solvent was exchanged three times, such that the total soaking time was 4 days. The methanol-exchanged crystals were then collected by filtration inside the glovebag. Anal. Calcd for $C_{228}H_{384}Cl_6Mn_{27}N_{192}O_{84}$: C, 30.93; H, 4.37; N, 30.37. Found: C, 30.91; H, 4.14; N, 30.67. IR (neat): 1618 (w, br), 1417 (s), 1230 (w), 1187 (w), 1016 (s), 901 (w), 789 (s), 751 (m), 698 (w) cm^{-1}. Crystals of **1m** become opaque and turn light yellow-brown in color upon prolonged exposure to the atmosphere and were therefore stored in sealed glass ampules. The desolvated form of the compound, $Mn_3[(Mn_4Cl)_3(BTT)_8(CH_3OH)_{10}]_2$ (**1m′**), was generated by heating **1m** at 150 °C under dynamic vacuum for a minimum of 2 h. Anal. Calcd for $C_{164}H_{128}Cl_6Mn_{27}N_{192}O_{20}$ (**1m′**): C, 28.95; H, 1.90; N, 39.52. Found: C, 28.46; H, 1.66; N, 39.13. IR (neat): 1587 (w, br), 1417 (s), 1236 (w), 1189 (w), 1015 (w), 790 (s), 751 (m), 692 (w) cm^{-1}.

Low-Pressure Gas Adsorption Measurements. Gas adsorption isotherms for pressures in the range 0−1.2 bar were measured using a Micromeritics ASAP2020 instrument. Samples of **1** and **1m** were transferred under a dinitrogen atmosphere to preweighed analysis tubes, which were then capped with a Transeal to prevent intrusion of oxygen and atmospheric moisture during transfers and weighing. The samples were evacuated by heating at 150 °C under dynamic vacuum until the outgas rate was less than 2 mTorr/min (0.27 Pa/min). The evacuated analysis tubes containing degassed samples were then carefully transferred to an electronic balance and weighed to determine the mass of sample (typically 50−200 mg). The tube was transferred back to the analysis port of the gas adsorption instrument. The outgas rate was again confirmed to be less than 2 mTorr/min (0.27 Pa/min). For all isotherms, warm and cold free space correction measurements were performed using ultra-high-purity He gas (UHP grade 5.0, 99.999% purity); H_2 and N_2 isotherms at 77 K were measured in liquid nitrogen baths using UHP-grade gas sources. H_2 isotherms at 87 K were measured in liquid argon baths. Oil-free vacuum pumps and oil-free pressure regulators were used for all measurements to prevent contamination of the samples during the evacuation process or of the feed gases during the isotherm measurement.

Derivation of the Isosteric Heats of Adsorption. A virial-type expression of the following form was used to fit the combined isotherm data for a given material at 77 and 87 K:

$$\ln P = \ln N + 1/T\sum_{i=0}^{m} a_i N^i + \sum_{i=0}^{n} b_i N^i \qquad (1)$$

Here, P is the pressure expressed in Torr, N is the amount adsorbed in mmol/g, T is the temperature in K, a_i and b_i are virial coefficients, and m and n represent the number of coefficients required to adequately describe the isotherms. The equation was fit using the **R** statistical software package;[30] m and n were gradually increased until the contribution of extra added a and b coefficients was deemed to be statistically insignificant toward the overall fit, as determined using the t-test. The values of the virial coefficients a_0 through a_m were then used to calculate the isosteric heat of adsorption using the following expression:

(26) Bhatia, S. K.; Myers, A. L. *Langmuir* **2006**, *22*, 1688−1700.
(27) Kaye, S. S.; Long, J. R. *J. Am. Chem. Soc.* **2005**, *127*, 6506−6507.
(28) Lochan, R. C.; Head-Gordon, M. *Phys. Chem. Chem. Phys.* **2006**, *8*, 1357−1370.
(29) Hill, M.; Mahon, M. F.; Molloy, K. C. *J. Chem. Soc., Dalton Trans.* **1996**, 1857−1865.
(30) Download, instructions, and further details on the use and capabilities of this software package area available online at http://www.r-project.org.

$$Q_{st} = -R\sum_{i=0}^{m} a_i N^i \quad (2)$$

Here, Q_{st} is the coverage-dependent isosteric heat of adsorption and R is the universal gas constant.

High-Pressure Gas Adsorption Measurements and Analysis. Crystals of **1** and **1m** were loaded into sample holders under an argon atmosphere. The samples were evacuated under a pressure of less than 10^{-4} Torr (0.013 Pa) in two stages: first heating at 40−50 °C for 5 h, and then at 150 °C for at least 10 h. Hydrogen excess adsorption analyses were performed using an automated controlled Sieverts' apparatus (PCT-Pro 2000 from Hy-Energy LLC) over a pressure range of 0−50 bar for **1′** and 0−90 bar for **1m′**. At least 300 mg of adsorbent was used in each experiment, and UHP-grade hydrogen and helium (99.999% purity) were used for all measurements. Volumetric measurements at 77 K were carried out by submerging the sample holder in a liquid nitrogen bath, for which the fill level was maintained constant throughout the experiment.

The volume of the sample holder and the connecting gas manifold was previously determined using H_2 and He at 298 K and at 77 K. Hydrogen was used to determine the dead-space volume correction for a nonporous sample of known volume; this correction accounted for the change in effective sample volume observed when cooling the sample holder from room temperature to 77 K. The adsorbent was then introduced into the sample holder, and He gas was used to determine the volume of the sample at room temperature. Since He gas penetrates the pores of the sample without being adsorbed onto the surface, the volume measured with He corresponds to the volume of the framework walls, also referred to as the framework skeleton. Consequently, the skeletal density of the material, d_{sk}, can be obtained from the following expression:

$$d_{sk} = m/V_{sk} \quad (3)$$

Here, m is the sample mass expressed in g, and V_{sk} is the sample volume in cm^3, as determined using He expansion at room temperature. In order to obtain an accurate assessment of the value of the skeletal density, the volume of the sample, V_{sk}, was measured 20 times, and the average of these was used as the final value.

Excess adsorption is defined as the amount of gas taken up by the surface of a porous adsorbent above and beyond the quantity of gas that would have occupied the adsorbent pore volume under the same temperature and pressure conditions in the absence of an adsorbent. The total storage capacity, however, is the sum of the capacity due to adsorption on the surface and the capacity due to compression within the void space of the pores of the adsorbent. The total adsorption capacity can therefore be expressed as follows:

$$C_{tot} = C_{exc} + \frac{100 \times d_g V_{pore}}{1 + d_g V_{pore}} \quad (4)$$

Here, C_{tot} is the total adsorption capacity expressed in weight percent (wt %), C_{exc} is the excess adsorption in wt % and is the quantity being measured, d_g is the density of the compressed gas (here H_2) at a given temperature and pressure in g/cm^3, and V_{pore} is the pore volume in cm^3/g.

In eq 4, the second term of the sum on the right-hand side represents the contribution of the compressed H_2 inside the pores to the total adsorption. Note that the denominator must contain the term $d_g V_{pore}$ for the capacity to be expressed in units of wt %. Omitting this term would correspond to units of grams of H_2 adsorbed per 100 g of adsorbent, and not to wt % of H_2 adsorbed. The compressed gas density, d_g, is the density of H_2 gas as a function of pressure at a given temperature. In the current experiments, the software package GasPak (v. 3.41) was used to plot the density of H_2 at 77 K as a function of pressure, as shown in Figure S8 (Supporting Information). If the bulk density of the sample, d_{bulk}, is known (typically, d_{bulk} is the crystallographic density of the sample), the pore volume can then be calculated as follows:

$$V_{pore} = \frac{d_{sk} - d_{bulk}}{d_{sk} d_{bulk}} \quad (5)$$

The volumetric density of H_2 adsorbed inside the sample can be obtained simply by multiplying the adsorbed quantity with the bulk density of the sample, d_{bulk}:

$$C_{vol} = Q_{ads} d_{bulk} \quad (6)$$

Here, C_{vol} is the volumetric H_2 capacity expressed in g/L, and Q_{ads} is the total quantity of H_2 taken up in mmol/g. The excess quantity of H_2 adsorbed may instead be used in this equation if "excess" volumetric capacity is the desired quantity.

X-ray Structure Determinations. Crystals of **1** and **1m′** were coated in Paratone-N oil, attached to Kapton loops, transferred to a Siemens SMART APEX diffractometer, and cooled in a dinitrogen stream. Lattice parameters were initially determined from a least-squares analysis of more than 100 centered reflections; these parameters were later refined against all data. None of the crystals showed significant decay during data collection. The raw intensity data were converted (including corrections for background, Lorentz, and polarization effects) to structure factor amplitudes and their esd's using the SAINT 4.15 program. An empirical absorption correction was applied to each data set using SADABS. Space group assignment was based on systematic absences, *E*-statistics, and successful refinement of the structures. Structures were solved by direct methods with the aid of difference Fourier maps and were refined against all data using the SHELXTL 5.0 software package. Hydrogen atoms were inserted at idealized positions and refined using a riding model with an isotropic thermal parameter 1.2 times that of the attached carbon atom. For **1**, thermal parameters for all non-hydrogen atoms in the framework skeleton and for the N and O atoms from bound DMF were refined anisotropically. The C atoms in each DMF molecule were disordered over four equivalent sites around the crystallographic 4-fold rotation axis and were consequently refined with 0.25 of their natural occupancies. All the interatomic distances in each DMF molecule were constrained to predefined values [O−$C_{carbonyl}$, 1.22(1) Å; $C_{carbonyl}$−N, 1.31(2) Å; N−C_{methyl}, 1.46(2) Å; C_{methyl}−C_{methyl}, 2.47(4) Å; $C_{carbonyl}$−C_{methyl}, 2.41-(3) Å] and refined as such. The van der Waals contacts between the C_{methyl} atoms of the DMF molecules and the Cl and N atoms in the framework lie between 3.8 and 4.0 Å. The coordination environment around the half-occupied Mn^{2+} was assigned to six DMF molecules using TGA and elemental microanalysis. Extensive disorder both locally, around the Mn^{2+} ion, and over neighboring unit cells prevents the refinement of any other atoms other than six O atoms disordered over 14 sites. Extra electron density in the pores was modeled as partially occupied oxygen atoms, with occupancies varying between 0.25 and 0.5 of the natural occupancy for a given set of crystal coordinates. For **1m′**, thermal parameters for all non-hydrogen atoms except for C and O in methanol molecules were refined anisotropically. Residual methanol molecules in the structure of **1m′** were disordered, and the total occupancy, including all disordered atoms, was refined best at 83.3% of the site occupancy. Hence, there is 0.83 of a methanol molecule for each Mn^{2+} site in the framework skeleton.

Neutron Diffraction Experiments. Neutron powder diffraction data were collected on the High Resolution Neutron Powder Diffractometer BT-1 at the NIST Center for Neutron Research (NCNR) with a Ge-(311) monochromator and using in-pile collimation of 15 min of arc, corresponding to a wavelength of 2.0787 Å. Measurements were taken as a function of deuterium loading at a temperature of 3.5 K with measurement times of ca. 9 h.

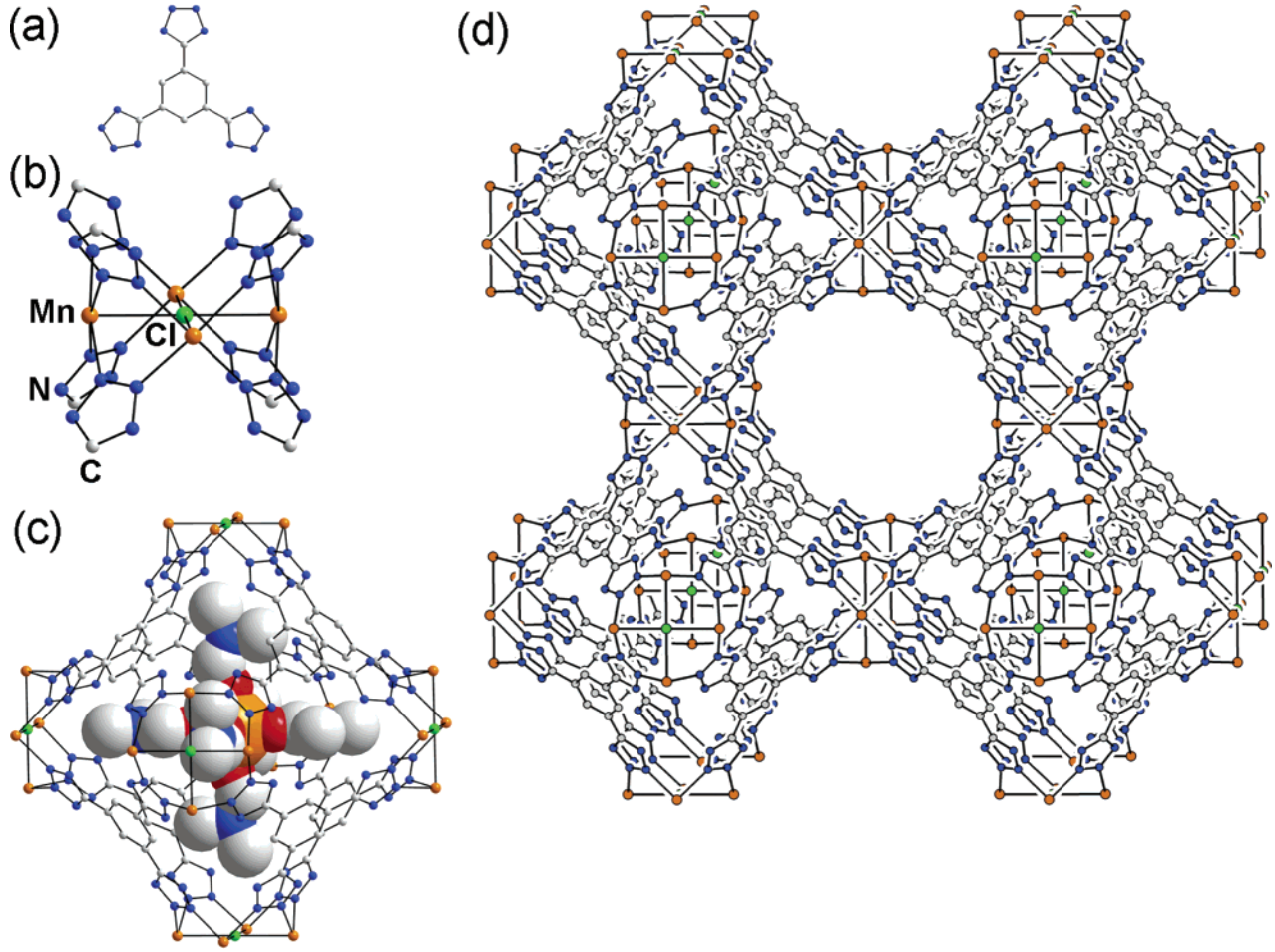

Figure 1. Portions of the crystal structure of **1**: (a) molecular structure of the tritopic ligand H_3BTT, (b) a square-planar Mn_4Cl cluster surrounded by eight tetrazolate rings, (c) a sodalite cage-like unit encasing a $[Mn(DMF)_6]^{2+}$ complex, and (d) a cube of eight such units sharing square Mn_4Cl faces. Hydrogen atoms and solvent molecules are omitted for clarity. Selected interatomic distances (Å) and angles (°): Mn−Cl 2.736(1), Mn−N 2.227(3), Mn···Mn 3.869(2), Mn−Cl−Mn 90.0, N−Mn−N 87.6(1), 91.4(1), Mn−N−N 125.3(2).

All sample transfers were performed in a helium-filled glovebox equipped with water and oxygen monitors. Initial sample activation was performed in a glass tube with a packless bellows valve attached. The sample was evacuated using a turbo pump (10^{-5} Torr) and heated to 150 °C with a ramp speed of ca. 1 °C per minute. After degassing at 150 °C for 24 h, the sample was cooled, pulverized using an agate mortar and pestle, transferred to a cylindrical vanadium can (i.d. = 0.95 cm) equipped with a capillary gas line and a packless valve, and sealed with a lead O-ring. The sample was mounted onto a sample stick equipped with a stainless-steel gas line with an additional valve for a top-loading closed-cycle helium refrigerator. The sample was further degassed in situ for ca. 20 min under high vacuum (8.5×10^{-7} to 7.5×10^{-6} Torr) at 150 °C. During the experiments, a known amount of hydrogen (deuterium) gas was loaded into the sample (907 mg), which was maintained at a temperature of 77 K until no pressure drop was observed for at least 1 min. The sample was then cooled down to the base temperature of 3.5 K over a period of 1 h in order to perform measurements. In all cases, the outgas pressure reading was zero well before reaching 25 K.

A diffraction pattern was collected for **1m′** prior to dosing with D_2. Subsequent Rietveld analysis indicated the existence of extra neutron density close to the Mn^{2+} ions in the framework skeleton, as expected due to the presence of residual methanol molecules. Accordingly, the extra neutron density was modeled using disordered O and C atoms, and this corrected "bare" model was used as a baseline for all subsequent measurements involving D_2. This extra scattering source proved to be absolutely necessary in order to achieve a low goodness-of-fit value for the bare material. The presence of methanol was confirmed by single-crystal X-ray diffraction[33] (see Figure S1), infrared spectroscopy (Figure S4), and elemental analysis. For X-ray diffraction, a single crystal was used, and, as such, modeling the disordered methanol molecules could be accomplished more easily. In contrast, the neutron powder diffraction experiments involved large amounts of powdered crystalline samples, and the methanol disorder in one crystallite may have differed from that in other crystallites, making it difficult to model the disorder over the entire sample. Consequently, partially occupied C and O atoms were introduced to account for the extra scattering densities in the bare material. In addition, owing to the extended disorder of the extraframework Mn^{2+} ions and to the small scattering factor of manganese, these ions could not be located using neutron diffraction; as such, their contribution to the fitted models was omitted.

Neutron scattering diffraction patterns were analyzed using the Rietveld refinement method.[31] The program EXPGUI was used to perform all refinements.[32] The model of the bare material was refined first, and it was used as the starting point for subsequent refinements of the D_2-loaded samples. Deuterium molecules are treated as point scatters with double occupancy since they are expected to be quantum mechanically spherically averaged in the ground state. As mentioned, during the refinement of the model for the bare material, extra C and O atoms were introduced to account for the scattering intensities from the residual methanol molecules bound to the intraframework Mn^{2+} ions. The information on the extra atoms was obtained from the

(31) Rietveld, H. M. *Acta Crystallogr.* **1967**, *22*, 151.
(32) Toby, B. H. *J. Appl. Crystallogr.* **2001**, *34*, 210.

diffraction pattern of the bare material and was fixed at these values when analyzing the cases with deuterium molecules loaded. The coordinates of all other atoms and the Debye−Waller factors were allowed to vary during the refinement of each deuterium loading case. Based on the structure obtained from the diffraction pattern of the bare material, the diffraction pattern of the case with 12 D_2/f.u. was analyzed by neglecting the D_2 molecules. The Fourier difference map was calculated and clearly indicated the positions of D_2 adsorption sites. Accurate values for the D_2 locations and occupancy numbers were then obtained by Rietveld refinement. For each successive D_2 loading, the Fourier difference map was calculated on the basis of the results of the previous D_2 loading and used to identify new D_2 adsorption sites.

Other Physical Measurements. Infrared spectra were collected on a Nicolet Avatar 360 FTIR spectrometer with an attenuated total reflectance accessory. ^{1}H NMR spectra were obtained using a Bruker AVQ-400 instrument. Carbon, hydrogen, and nitrogen analyses were obtained from the Microanalytical Laboratory of the University of California, Berkeley. Thermogravimetric analyses were carried out at a ramp rate of 1 °C/min in a nitrogen flow with a TA Instruments TGA 2950. X-ray powder diffraction data were collected using Cu Kα ($\lambda = 1.5406$ Å) radiation on a Siemens D5000 diffractometer. Prior to collecting X-ray powder diffraction data, the as-synthesized sample was ground using an agate mortar and pestle.

Results and Discussion

Reaction of H_3BTT with $MnCl_2 \cdot 4H_2O$ in an acidic solution of *N*,*N*-dimethylformamide (DMF) and methanol at 70 °C afforded cube-shaped crystals of $[Mn(DMF)_6]_3[(Mn_4Cl)_3(BTT)_8(H_2O)_{12}]_2 \cdot 42DMF \cdot 11H_2O \cdot 20CH_3OH$ (**1**) in 40% yield. X-ray analysis[33] of a crystal of **1** revealed a cubic structure in which chloride-centered square-planar $[Mn_4Cl]^{7+}$ units are linked via BTT^{3-} ligands to form the anionic, three-dimensional framework shown in Figure 1. The N2 and N3 atoms of two tetrazolate rings on individual BTT^{3-} ligands bridge pairs of Mn^{2+} ions along the edges of a square, such that each $[Mn_4Cl]^{7+}$ moiety is surrounded by eight BTT^{3-} ligands. In turn, each BTT^{3-} ligand connects three $[Mn_4Cl]^{7+}$ units so that, overall, six squares and eight planar BTT^{3-} ligands define the faces of a truncated octahedron, reminiscent of a sodalite cage. Each cage shares its square faces with six neighboring cages, defining a network structure closely related to that of sodalite.[34] Alternatively, the square-planar $[Mn_4Cl]^{7+}$ units surrounded by eight tetrazolates can be considered as tetragonally distorted 8-connected nodes that, together with the trigonal planar nodes presented by the BTT^{3-} ligands, define a three-dimensional 3,8-connected net (see Figure 2). Notably, this is the first example of a compound displaying such a "Moravia" net, the existence of which was only recently predicted by theory.[35] Within the anionic framework skeleton, formulated as $[(Mn_4Cl)_3(BTT)_8(H_2O)_{12}]^{3-}$, water ligands occupy the sixth coordination site on each Mn^{2+} ion, while charge balance is provided by $[Mn(DMF)_6]^{2+}$ complexes situated inside both the sodalite cage-like units and the larger three-dimensional cavities formed by eight such units. Note that a single $[Mn(DMF)_6]^{2+}$ complex fits snugly within a cage, suggesting that it may in fact act as a template for the in situ formation of the framework.

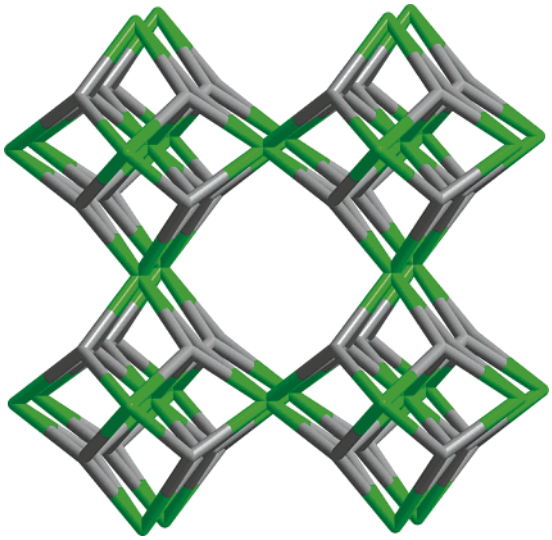

Figure 2. 3,8-Connected three-dimensional net derived from the structure of **1**. Gray 3-connected nodes represent BTT^{3-} ligands, while green 8-connected nodes represent square-planar Mn_4Cl clusters surrounded by eight tetrazolate rings, as depicted in Figure 1a and b, respectively.

Thermogravimetric analysis of **1** showed a weight loss of 22.0% up to 160 °C, suggesting that methanol, water, and some DMF molecules are evacuated at this temperature (21.9% expected for 20 methanol, 35 water, and 18 DMF molecules). Framework decomposition, observed above 200 °C, precluded evacuation of the remaining 42 DMF molecules, which were expected to occupy all 18 coordination sites on the extraframework cations and all 24 sites on the intraframework cations, thus prohibiting access to unsaturated Mn^{2+} centers and reducing the accessible surface area. To attain a more complete evacuation, DMF was exchanged with methanol by soaking crystals of **1** in methanol for 4 days. While other organic solvents can be exchanged inside the framework, methanol was chosen for its relatively low boiling point and ease of potential removal via evacuation. As indicated by infrared spectroscopy and elemental analysis, the resulting material is water- and DMF-free, with formula $[Mn(CH_3OH)_6]_3[(Mn_4Cl)_3BTT_8(CH_3OH)_{12}]_2 \cdot 42CH_3OH$ (**1m**). Thermogravimetric analysis of **1m** showed a weight loss step below 100 °C, corresponding to methanol loss, followed by a plateau between 100 and 200 °C, beyond which framework decomposition occurred.

Remarkably, crystals of **1m** remained single upon heating to 150 °C, enabling a crystal structure determination for the desolvated compound.[33] Here, X-ray analysis revealed an intact framework skeleton, with some residual methanol (20 molecules per formula unit). The charge-balancing, extraframework Mn^{2+} ions, initially complexed by DMF in **1**, are now ligated by the N1 and N4 atoms of adjacent tetrazole rings and are disordered over 24 symmetry-equivalent positions (see Figure S1). The residual methanol molecules coordinate 83% of the framework Mn^{2+} ions, leaving a small fraction of these metal centers with open coordination sites. Despite numerous attempts, evacuation conditions for removing all of the remaining methanol without degrading the framework have not yet been discovered.

The partially desolvated forms of **1** and **1m**, denoted **1′** and **1m′**, adsorb significant amounts of N_2: 310 and 550 cm^3/g, respectively, with both displaying type I adsorption isotherms

(33) Crystal and structure refinement parameters for **1**: $T = 166$ K, space group $Pm\bar{3}m$, $Z = 2$, $a = 19.116(1)$ Å, $V = 6985.2(7)$ Å^3, $R_1 = 0.0771$, w$R_2 = 0.2508$. For **1m′**: $T = 161$ K, $Pm\bar{3}m$, $Z = 2$, $a = 19.009(1)$ Å, $V = 6868.3(7)$ Å^3, $R_1 = 0.0486$, w$R_2 = 0.1417$.

(34) Wells, A. F. *Three-dimensional nets and polyhedra*; Wiley: New York, 1977.

(35) Bucknum, M. J.; Castro, E. A. *Central Eur. J. Chem.* **2005**, *3*, 169−173.

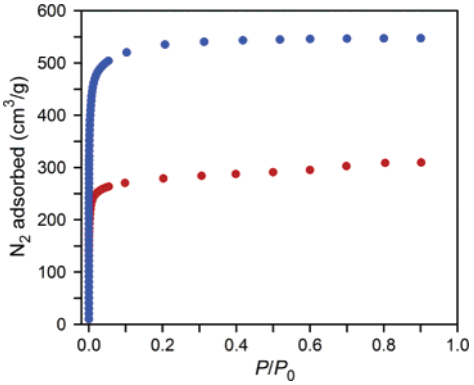

Figure 3. Isotherms for the adsorption of N_2 within **1′** (red) and **1m′** (blue) at 77 K.

typical of a microporous material (see Figure 3).[36] Fitting the BET equation to the N_2 isotherms gave estimated surface areas of 1100 and 2100 m^2/g for **1′** and **1m′**, respectively. For comparison, crystalline zeolites and activated carbons can have surface areas of up to 904 and 2800 m^2/g, respectively.[37,38] The highest surface area yet reported for a microporous metal−organic framework is 5900 m^2/g,[39] although most values fall below 1000 m^2/g.[40] Note that replacement of the DMF molecules with methanol, followed by evacuation at 150 °C, results in almost a doubling of the available surface area, suggesting that H_2 adsorption should also be enhanced in **1m′** relative to **1′**.

The hydrogen storage properties of **1′** and **1m′** were evaluated using volumetric gas adsorption measurements. The resulting isotherms, depicted in Figure 4a, show fully reversible uptakes of 1.7 wt % in **1′** and 2.2 wt % in **1m′** at 77 K and 1.2 bar. The excess H_2 adsorption, defined as the amount of H_2 adsorbed in excess of the bulk gas that would occupy the pores of the adsorbent,[41] reaches 2.8 wt % in **1′** and 5.1 wt % in **1m′** at saturation, as shown in Figure 4b. A more informative quantity for practical applications, however, is the total H_2 uptake, which is defined simply as the total amount stored in the bulk volume of the adsorbent, as determined using the crystallographic density of the material (see Table S2). Thus, within a fuel tank maintained at 77 K, the materials are expected to show total uptakes of 3.9 wt % for **1′** at 50 bar and 6.9 wt % for **1m′** at 90 bar. Note that a higher gravimetric capacity has recently been reported for Zn_4O(1,3,5-benzenetribenzoate)$_2$, which exhibits an excess adsorption of 7.0 wt % and is expected to exhibit an even higher total adsorption at 60 bar and 77 K.[18]

Together with the weight requirements, H_2 storage in mobile applications imposes limitations with respect to the tank volume. Volumetric capacity thus becomes a critical parameter when comparing different storage materials. Significantly, the excess volumetric adsorption in **1m′** reaches 43 g/L at 90 bar and 77 K, 9 g/L higher than that observed within Zn_4O(1,3,5-benzenetribenzoate)$_2$,[18] while the total volumetric uptake reaches 60 g/L. The latter value is only 11 g/L lower than the density of liquid hydrogen (71 g/L at 1 bar and 20 K), suggesting the possibility of converting existing liquid hydrogen-based storage systems for use with a liquid nitrogen coolant. We attribute this high volumetric storage density to the relatively compact nature of the metal−organic framework and, as discussed below, a reduction in the volume taken up by the strongly adsorbed H_2 molecules.

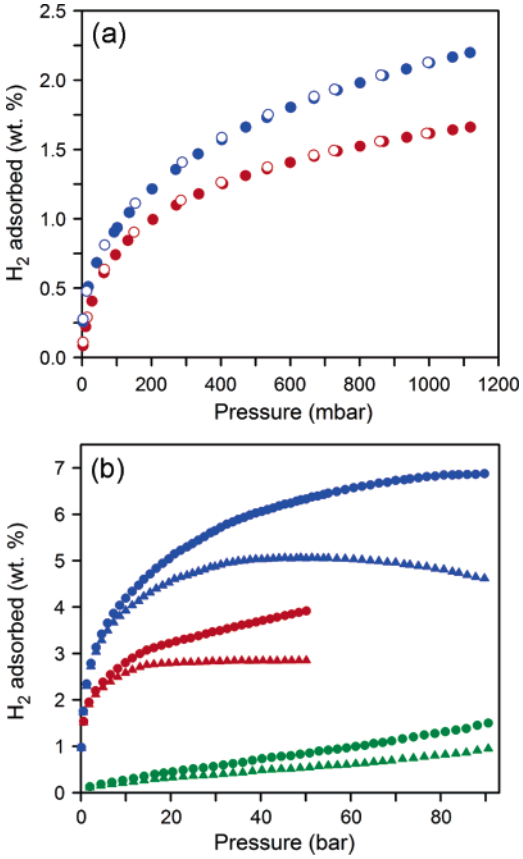

Figure 4. H_2 adsorption isotherms (a) below 1.2 bar and (b) up to 90 bar within **1′** (red) and **1m′** (blue) at 77 K, and within **1m′** at 298 K (green). Triangles and circles represent excess and total H_2 adsorption, respectively, while filled and open symbols represent adsorption and desorption data, respectively.

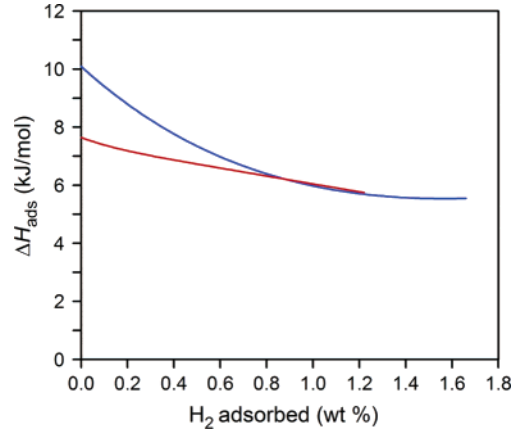

Figure 5. Isosteric heat of adsorption curves for H_2 uptake in **1′** (red) and **1m′** (blue).

To probe how the presence of open Mn^{2+} coordination sites influences the binding enthalpy, H_2 adsorption isotherms in the range 0−1.2 bar were also measured at 87 K. The 77 and 87 K

(36) Sing, K. S. W.; Everett, D. H.; Haul, R. A. W.; Moscou, L.; Pierotti, R. A.; Rouquérol, J.; Siemieniewska, T. *Pure Appl. Chem.* **1985**, *57*, 603−619.
(37) Chester, A. W.; Clement, P.; Han, S. U.S. Patent 2000/6,136,291A.
(38) Gregg, S. G.; Sing, K. S. W. *Adsorption, Surface Area and Porosity*; Academic Press: New York, 1982.
(39) Férey, G.; Mellot-Draznieks, C.; Serre, C.; Millange, F.; Dutour, J.; Surblé, S.; Margiolaki, I. *Science* **2005**, *309*, 2040−2042.
(40) Janiak, C. *Dalton Trans.* **2003**, 2781−2804.
(41) Menon, P. G. *Chem. Rev.* **1968**, *68*, 277−294.
(42) Czepirski, L.; Jagiello, J. *Chem. Eng. Sci.* **1989**, *44*, 797−801.

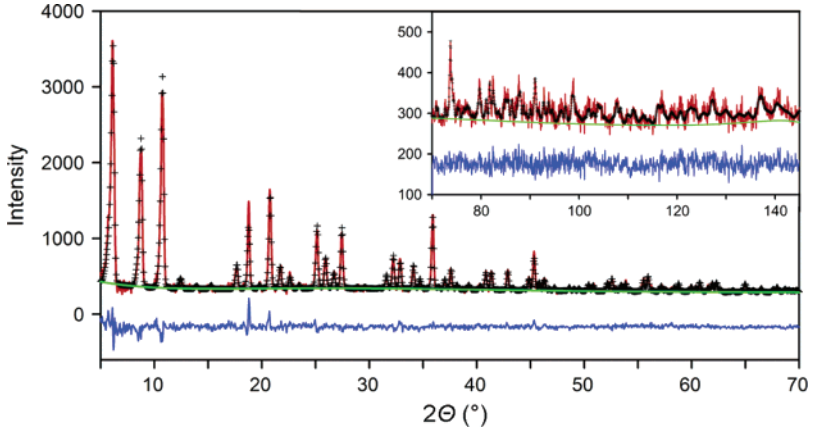

Figure 6. Rietveld refinement of neutron powder diffraction data for a loading of 12 D_2 molecules per formula unit of **1m′**. Green lines, crosses, and red lines represent the background, calculated, and experimental diffraction patterns, respectively. The blue line shows the difference between experimental and calculated patterns. The final Rietveld fit parameter was $\chi^2 = 0.985$.

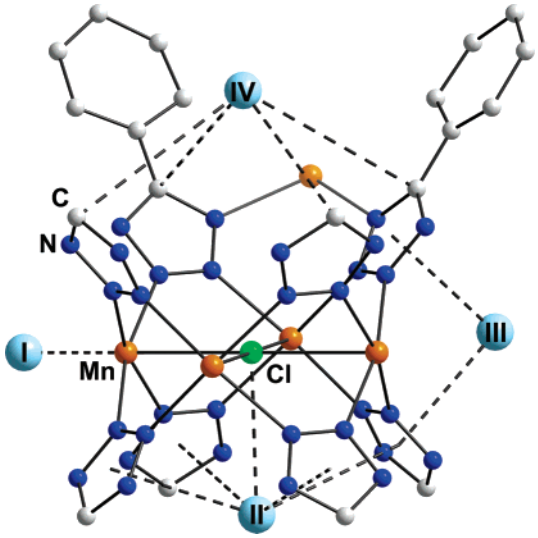

Figure 7. Initial D_2 adsorption sites within **1m′**. Light blue spheres represent D_2 centroids, while the transparent orange sphere shows the position of a partially occupied, extraframework Mn^{2+} ion site. Hydrogen atoms and methanol molecules are omitted for clarity.

isotherms were then fit using a virial equation[42] of the type previously used to model adsorption in microporous materials with heterogeneous pore surfaces.[21,43,44] Virial coefficients obtained from the fits were then employed in calculating the isosteric heats of adsorption for the two evacuated materials. The ensuing enthalpies lie in the range 5.7−7.6 kJ/mol for **1′**, depending on degree of H_2 loading, while for **1m′** the upper limit increases to 10.1 kJ/mol (see Figure 5). This represents the highest value reported for a metal−organic framework.[15,21] Notably, the heat of adsorption curves for **1′** and **1m′** show a large gap at low H_2 coverages and then overlay at coverages above ca. 0.8 wt %. Thus, strong H_2 adsorption sites become available in **1m′** that are not present in DMF-passivated **1′**.

Neutron powder diffraction experiments[45] were performed as a direct check of whether the high binding enthalpy in **1m′** is associated with coordination of H_2 at exposed Mn^{2+} sites. Figure 6 shows the diffraction pattern observed at 3.5 K upon adsorption of 12 D_2 molecules per formula unit. Using a Rietveld profile analysis, the two strongest binding sites at this low loading could be associated with sites I and II in Figure 7. Significantly, site I is located just 2.27 Å from the Mn^{2+} ions in the framework skeleton, providing the first neutron diffraction evidence for a metal−H_2 interaction within a metal−organic framework.[46] To our knowledge, this is the first example of H_2 binding to a Mn^{2+} ion, although many examples of H_2 binding to Mn^{+} complexes and other transition metal species exist.[47−50] The D_2 molecules at site II are situated inside the sodalite-like cages and exhibit van der Waals contacts of 3.47 and 3.66 Å with a chloride anion and four equidistant tetrazolate rings, respectively. The sum of the five corresponding attractive interactions is likely responsible for a significant adsorption enthalpy at this site as well. Indeed, when the total D_2 loading is increased to 48 molecules per formula unit, site II becomes fully occupied.

Increased D_2 loadings also permitted identification of the next strongest binding site, labeled III, and a possible binding site labeled IV in Figure 7. The D_2 molecules at site III are situated inside the larger framework cavities and have van der Waals contacts of 3.26 Å with two equidistant tetrazole rings. At site IV, only 5 D_2 molecules could be identified; these are located inside the smaller cavities, and are in closest contact (4.72 Å) with four carbon atoms from neighboring tetrazolate rings. Out of 48 D_2 molecules refined from a model derived from the difference scattering length map, 7.0 reside at site I, 10.7 at site II, 23.9 at site III, and 5.0 at site IV. Importantly, the H_2 uptake corresponding to complete filling of sites I and II is 0.6 wt %, coinciding with the region where heat of adsorption curves for **1′** and **1m′** separate, as shown in Figure 5. This demonstrates that the two strongest H_2 binding sites are indeed likely responsible for the increase in binding energy upon going from

(43) Ansón, A.; Jagiello, J.; Parra, J. B.; Sanjuán, M. L.; Benito, A. M.; Maser, W. K.; Martínez, M. T. *J. Phys. Chem. B* **2004**, *108*, 15820−15826.
(44) Jagiello, J.; Bandosz, T. J.; Putyera, K.; Schwarz, J. A. *J. Chem. Eng. Data* **1995**, *40*, 1288−1292.
(45) Similar experiments enabled, for example, identification of the H_2 binding sites within Zn_4O(1,4-benzenedicarboxylate)$_3$: Yildirim, T.; Hartman, M. R. *Phys. Rev. Lett.* **2005**, *95*, 215504(1−4.).
(46) Very recently, a report appeared providing the first infrared spectroscopic evidence for H_2 coordinating a metal site within a metal−organic framework: Prestipino, C.; Regli, L.; Vitillo, J. G.; Bonino, F.; Damin, A.; Lamberti, C.; Zecchina, A.; Solari, P. L.; Kongshaug, K. O.; Bordiga, S. *Chem. Mater.* **2006**, *18*, 1337−1346.
(47) Sweany, R. L.; Watzke, D. *Organometallics* **1997**, *16*, 1037−1042.
(48) Toupadakis, A.; Kubas, G. J.; King, W. A.; Scott, B. L.; Huhmann-Vincent, J. *Organometallics* **1998**, *17*, 5315−5323.
(49) Kubas, G. J.; Ryan, R. R.; Swanson, B. I.; Vergamini, P. J.; Wasserman, H. J. *J. Am. Chem. Soc.* **1984**, *106*, 451−452.
(50) Kubas, G. J. *Metal Dihydrogen and σ-Bond Complexes*; Kluwer Academic/Plenum Publishers: New York, 2001.

1′ to **1m′**. Experiments intended to locate weaker adsorption sites and to determine the rotational potential dynamics at the H_2 adsorption sites (using inelastic neutron scattering) are underway.

Outlook

A key and challenging aspect of hydrogen storage research is the ability to control the H_2 binding energy, which governs the adsorption in materials ranging from microporous solids to metal hydrides. In this regard, a very attractive property of metal−organic frameworks is that their pores can be engineered at the atomic scale, thereby enabling some control over the H_2 binding interaction. The foregoing results show that, on a materials characteristic basis, metal−organic frameworks with unsaturated metal centers can exceed the 2010 DOE H_2 storage targets of 6.0 wt % and 45 g/L.[2] Meeting these targets for a complete storage *system*, however, will require further efforts toward raising the H_2 binding energy, such that storage at closer to ambient conditions can be accomplished. Ultimately, this may be possible in materials related to those reported here through adjustment of the electronic structure of the metal ions and exposure of a higher concentration of coordination sites.

Acknowledgment. This research was funded by the General Motors Corp. Work at NIST was partially supported by the U.S. DOE within the Center of Excellence for Carbon-Based Hydrogen Storage Materials. The ITRI/Berkeley Research Center is also acknowledged for providing a predoctoral fellowship for M.D. We thank Dr. Scott W. Jorgensen, Dr. Frederick J. Hollander, Alexandra I. Gliga, and Fernando D. Hidalgo for helpful discussions. We also thank Juscelino Leo and Judy Stalick for support with the neutron diffraction experiments.

Supporting Information Available: Full table of X-ray refinement statistics, tables of refinement statistics and atomic parameters from neutron diffraction, tables of gas adsorption data, further views of the crystal structure of **1m′**, thermogravimetric analysis plots for **1** and **1m′**, additional plots of isotherm data and plots of the virial fits including the values of virial coefficients a_i and b_i, powder X-ray diffraction patterns for **1**, a Fourier difference neutron density map for the case of 12 D_2/f.u., and the structure of **1m′** as determined using neutron powder diffraction (PDF); X-ray crystallographic files (CIF). This material is available free of charge via the Internet at http://pubs.acs.org.

JA0656853